Journal of Hazardous Materials 514 (2026) 142964

Contents lists available at ScienceDirect

Journal of Hazardous Materials

journal homepage: www.elsevier.com/locate/jhazmat

Fuel-governed structure trait and emission potential of environmentally persistent free radicals from coking and metallurgical industry zones

Chenxu Gao [a], Shunyu Ding [a], Xiaoyao Ma [a], Jiangyao Chen [a,b,*]

[a] Guangdong Key Laboratory of Environmental Catalysis and Health Risk Control, Guangdong Technology Research Center for Photocatalytic Technology Integration and Equipment Engineering, Institute of Environmental Health and Pollution Control, Guangdong University of Technology, Guangzhou 510006, China
[b] Guangzhou Key Laboratory of Environmental Catalysis and Pollution Control, Guangdong-Hong Kong-Macao Joint Laboratory for Contaminants Exposure and Health, School of Environmental Science and Engineering, Guangdong University of Technology, Guangzhou 510006, China

HIGHLIGHTS

- Coking EPFR concentration is an order of magnitude higher than metallurgy one.
- Fuel dominates the formation and properties of EPFRs from Coal industry zone.
- Fly ash yield gap is the core driver of differential atmospheric EPFR emissions.
- Thermal and light treatment effect EPFR concentration rather than g-factor or $\Delta H_{p\text{-}p}$.
- The g-factor or $\Delta H_{p\text{-}p}$ is a stable tracer for atmospheric EPFR source identification.

GRAPHICAL ABSTRACT

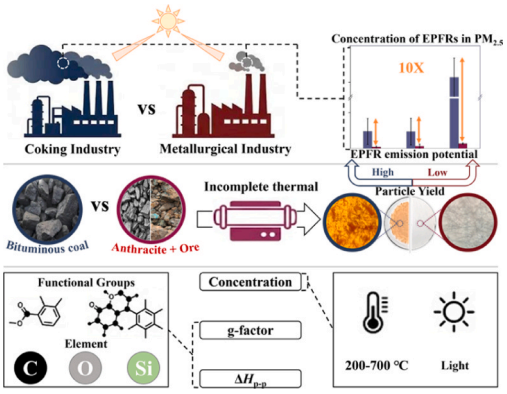

ARTICLE INFO

Keywords:
Coal combustion
Industry technique
Persistent free radicals
Emission characteristics
Migration and transformation

ABSTRACT

Coal-based industrial thermal treatment processes are dominant sources of $PM_{2.5}$-bound environmentally persistent free radicals (EPFRs), yet emission characteristics from pure coal versus coal-ore mixed sources remain unclear. Here, field measurements in coking and metallurgical industry zones coupled with laboratory simulations (bituminous coal vs. anthracite; thermal/light treatments) were conducted to elucidate structural trait and emission potential of EPFRs. Field data revealed that concentration of EPFRs in coking zone was an order of magnitude higher than that in metallurgy zone, dominated by carbon-centered and oxygen-centered radicals, respectively. Laboratory simulations demonstrated that the 6.5-fold higher fly ash yield of bituminous coal over anthracite under 500 ℃ thermal treatment drove this disparity, confirming that fuel governed the emission potential of EPFRs. Thermal treatment temperature and light intensity affected EPFR concentration, but did not alter the g-factors and $\Delta H_{p\text{-}p}$, which were intrinsically determined by the fuel. These conclusions were further validated through correlation analyses associating $PM_{2.5}$ components (C, O, C═O, Ca, Si) from both zones with EPFR g-factors and $\Delta H_{p\text{-}p}$. Comprehensive analysis confirmed that the coking zone output EPFRs to the

* Corresponding author at: Guangdong Key Laboratory of Environmental Catalysis and Health Risk Control, Guangdong Technology Research Center for Photocatalytic Technology Integration and Equipment Engineering, Institute of Environmental Health and Pollution Control, Guangdong University of Technology, Guangzhou 510006, China.
E-mail address: chenjiangyao@gdut.edu.cn (J. Chen).

https://doi.org/10.1016/j.jhazmat.2026.142964
Received 1 May 2026; Received in revised form 22 June 2026; Accepted 8 July 2026
Available online 9 July 2026

surrounding environment, while metallurgical zone EPFRs were driven by exogenous mixed sources. This work provides a scientific basis for the source apportionment and control of industrial EPFRs.

1. Introduction

Coal, as a foundational fossil fuel, underpins global energy and heavy chemical industries [1], supplying 35% of global electricity in 2024 and meeting over 85% of energy and coke demand for China's steel sector [2,3]. Industrial coal utilization falls into two distinct systems, including pure coal thermal treatment processing represented by coking [4] and coal-ore mixed thermal treatment processing represented by metallurgy [5,6]. Coal rank selection depends on industrial demands for calorific value, carbon content, and economic cost. Bituminous coal with high volatile matter serves as the primary fuel for coking and power generation [3], while anthracite characterized by high fixed carbon and low reactivity is preferred for metallurgical smelting, as its high carbon content and low volatile matter content are critical for blast furnace reduction reactions [7]. While critical to global industrial infrastructure, coal thermal treatment processing is a dominant anthropogenic source of atmospheric fine particulate matter [8], hazardous organics, and heavy metals [9,10]. Stringent environmental regulations have drastically reduced conventional pollutant emissions from coal-intensive regions via widespread desulfurization, denitrification, and high-efficiency dust removal technologies [11–13], shifting global research focus to emerging persistent pollutants with long environmental lifetimes and high chemical reactivity.

Among emerging persistent pollutants, environmentally persistent free radicals (EPFRs) have become as a critical research focus in atmospheric chemistry and environmental toxicology [14]. These particle-bound stable radicals exhibit half-lives ranging from days to months [15,16], and their strong oxidative activity triggers excessive reactive oxygen species generation in biological systems [17,18], posing substantial, well-documented risks to atmospheric quality and human respiratory health [19]. Previous mechanistic studies have revealed distinct EPFR formation pathways. The coking generating carbon-centered radicals dominated by bituminous coal organic precursors [20,21], while metallurgical forms mixed carbon and oxygen-centered radicals via interactions between coal organics and ore-derived transition metals [22–24]. Despite these different mechanistic insights, a critical knowledge gap remains. Direct comparative evidence for divergent EPFR emission characteristics between pure coal and coal-ore mixed industrial systems is still lacking, which hinders the development of accurate source apportionment methods and source-specific pollution control strategies for atmospheric EPFRs.

The formation and environmental behavior of coal-derived EPFRs are jointly regulated by fuel, thermal treatment conditions, and environmental factors [25]. Fuel properties (coal rank, organic functional groups, elemental distribution) fundamentally determine EPFR structural traits (g-factor and $\Delta H_{p\text{-}p}$) by dictating pyrolytic radical intermediates [26–28]. For example, the biomass pyrolysis tends to generate oxygen-centered radicals (10^{14}–10^{18} spins g^{-1}) [29–31], whereas coal thermal promotes higher concentrations of carbon-centered radicals (10^{17}–10^{20} spins g^{-1}) [30,32,33], via organic precursor-transition metal synergies [9,26,34]. Thermal treatment conditions govern EPFR formation efficiency, the moderate temperatures (400–600 ℃, incomplete thermal treatment) optimize EPFR formation; over 700 ℃ induces radical quenching, and below 400 ℃ limits pyrolysis [31,35,36]. Environmental factors (e.g., light irradiation triggering concentration fluctuations, particle-bound transition metals enhancing stability) also modulate post-emission EPFR concentration dynamics [27,32,37,38]. However, existing studies focus on single factors or isolated processes, lacking systematic cross-industrial EPFR characteristic comparisons and validation of the three factors synergistic effects under realistic conditions.

To address these critical knowledge gaps, this study selected coking (pure bituminous coal) and metallurgy (anthracite-copper ore mixtures) as representative coal-based industries. Integrating industrial z1 $PM_{2.5}$ field observations, lab thermal treatment simulations and photochemical aging experiments, we systematically characterized key EPFR parameters (concentration, g-factor, $\Delta H_{p\text{-}p}$) and carrier particle physicochemical properties. We aimed to compare the two industries source-specific EPFR emission characteristics, elucidate synergistic mechanisms of fuel and thermal conditions governing initial EPFR formation, unravel light irradiation effects on post-emission EPFR evolution, verify EPFR structural parameters as source tracers, and provide a scientific basis for targeted EPFR risk assessment and emission control.

2. Materials and methods

2.1. Sampling sites and methods

Atmospheric $PM_{2.5}$ sampling was conducted in October 2020 and November 2021. Two industry-specific representative sites were selected for this study, including a large-scale coking industrial in Lvliang City, Shanxi Province, and a typical metallurgical industrial in Daye City, Hubei Province. The two industrial zones are separated by more than 1000 km, with no overlapping atmospheric transport pathways for industrial pollutants. Both sampling campaigns were conducted in autumn and winter under typical stable atmospheric conditions, with similar meteorological backgrounds in terms of temperature (0–15 ℃) and wind speed regimes (Beaufort scale 1–2). The coking process in this study is dominated by oxygen-deficient incomplete pyrolysis of bituminous coal, while the metallurgical process involves high-temperature incomplete combustion of anthracite for ore smelting reduction, both of which are classified as typical industrial coal thermal treatment processes (Fig. S1).

In the coking industrial (112.206°−112.296°E, 37.541°−37.583°N), 11 sampling points were established. In the metallurgical industrial (114.542°−114.565°E, 30.093°−30.113°N), 10 sampling points were deployed (Table S1). The sampling method for $PM_{2.5}$ is described in **Appendix A Text S1–1.1**. Based on their distance from the plant area, the sampling points were categorized into three zones: < 1 km (C1, M1), 1–2 km (C2, M2), and > 2 km (C3, M3), where C and M denote Coking and Metallurgy, respectively (Fig. 1**A**). This study focused on capturing the spatial distribution characteristics of EPFRs around industrial zones, therefore adopted a multi-site spatial coverage strategy rather than replicate sampling at a single site. This design better reflects the spatial heterogeneity of industrial emissions within the 2 km buffer zone. Particulate matter within 2 km is dominated by primary industrial emissions, which preserves the original chemical fingerprints of the emission sources. Meanwhile, this distance minimizes the combined interference from long-range transport, atmospheric aging, and secondary transformation.

2.2. Laboratory thermal treatment emission and photochemical aging experiments

Coking and metallurgical industrial processes were simulated in a tube furnace system under strictly consistent conditions, with raw material composition as the only variable. For coking simulation, standard bituminous coal (GBW−11101) was used as the sole feedstock to replicate the oxygen-deficient bituminous coal pyrolysis core of industrial coking. For metallurgical simulation, standard anthracite (GBW−11126) blended with basic copper carbonate (5–15 wt%) was used to simulate high-temperature coal-ore smelting, with the gradient

designed to isolate the influence of ore components on EPFR characteristics. Synchronous blank control experiments were conducted for all batches to eliminate background interference. All pyrolysis solid products (cinder and fly ash) were collected, light-protected, and stored at −20 °C until testing.

Atmospheric photochemical aging of pyrolysis residues was performed in a sealed reaction chamber equipped with 365 nm black light lamps. To ensure experimental reliability, the black light lamps were verified using a spectrometer (Fig. S2). Homogenized and sieved cinder were evenly exposed to controlled UV irradiation for set durations. Post-reaction samples were immediately sealed, light-protected, and stored at −20 °C for subsequent analysis.

Full details of experimental operating parameters, instrument specifications, and quality control protocols are provided in the **Appendix A Text S1–1.2**.

2.3. Analytical Methods for $PM_{2.5}$ and EPFRs

The mass concentration of atmospheric $PM_{2.5}$ was determined following the standard gravimetric method specified in U.S. EPA 40 CFR Part 50 Appendix L (**Appendix A Text S1–1.3**) [39]. The mass of filters before and after sampling was recorded as m_1 and m_2, respectively, and V represents the volume of sampled air converted to standard conditions (0 ℃, 101.325 kPa, m^3). The mass concentration of $PM_{2.5}$ (C, μg m^{-3}) was calculated as follows:

$$C = \frac{m_2 - m_1}{V} \times 1000 \quad (1)$$

Electron paramagnetic resonance (EPR) spectroscopy (Bruker EMXplus−10/12) was used to directly detect EPFRs. All EPR measurements were completed within 30 days after sample collection/preparation, and all samples were sealed and stored at −20 °C in the dark throughout the period. The g-factor and ΔH_{p-p}, which serve as critical parameters for the characterization of the EPFRs, were analyzed using WinEPR software [27,40]. The ΔH_{p-p} was directly measured from the first-derivative EPR spectra, defined as the magnetic field distance between the maximum and minimum peaks of the first-derivative signal. All spectra in this study exhibited predominantly Lorentzian line shapes. The g-factor was calculated using the following formula, where v is the actual test frequency (GHz) and B is the magnetic field intensity (G):

$$g = \frac{714.4773 \times v}{B} \quad (2)$$

The morphology of $PM_{2.5}$, raw coal, and coal cinder samples was observed via optical microscopy and scanning electron microscopy (SEM), the functional group characteristics were analyzed using Fourier transform infrared spectroscopy (FTIR), and the elemental composition was determined via energy dispersive X-ray spectroscopy (EDS) and X-ray fluorescence spectroscopy (XRF). The detailed information on all characterization methods used in this study is provided in **Appendix A Text S1–1.4**.

3. Results and discussion

3.1. Characteristics of $PM_{2.5}$ and EPFRs in coking and metallurgical industry zones

This section analyzes EPFRs in $PM_{2.5}$ collected within a 2-km radius of coking and metallurgical industry zones (sampling details are provided in 2.1, Fig. 1**A** and Table S1). As illustrated in **Figs. 1B** and **S3**, the mass concentrations of $PM_{2.5}$ in the coking and metallurgical industry zones ranged from 33.35 to 255.88 μg m^{-3} and 43.13–154.47 μg m^{-3}, respectively. These results are consistent with $PM_{2.5}$ concentrations reported around coking [41] and metallurgical [42] industries in previous studies, reflecting typical industrial emission characteristics. The concentration ranges of EPFRs in the two zones (Fig. 1**C** and **S3**) were 0.15–58.82 × 10^{18} spins g^{-1} and 0.24–7.44 × 10^{17} spins g^{-1}, respectively. The results indicate that both $PM_{2.5}$ and EPFRs loads emitted from the coking industry zone were significantly higher than those from the metallurgical industry zone, with EPFR concentrations differing by approximately one order of magnitude. The g-factor is governed by spin-orbit coupling, reflecting the chemical environment and atomic identity of the unpaired electron host. Higher g-values indicate stronger contributions from heteroatoms (e.g., oxygen-centered radicals) relative to pure carbon-centered radicals. Figs. S4-S6 indicate that the g-factor of EPFRs in the coking and metallurgical industry zones ranged from 2.0022 to 2.0030 and 2.0021–2.0042, respectively. The EPFRs in the coking zone exhibited relatively low and narrow-range g-factors, indicating that they were dominated by typical carbon-centered radicals [43]. In contrast, the EPFRs in the metallurgical zone showed a wider

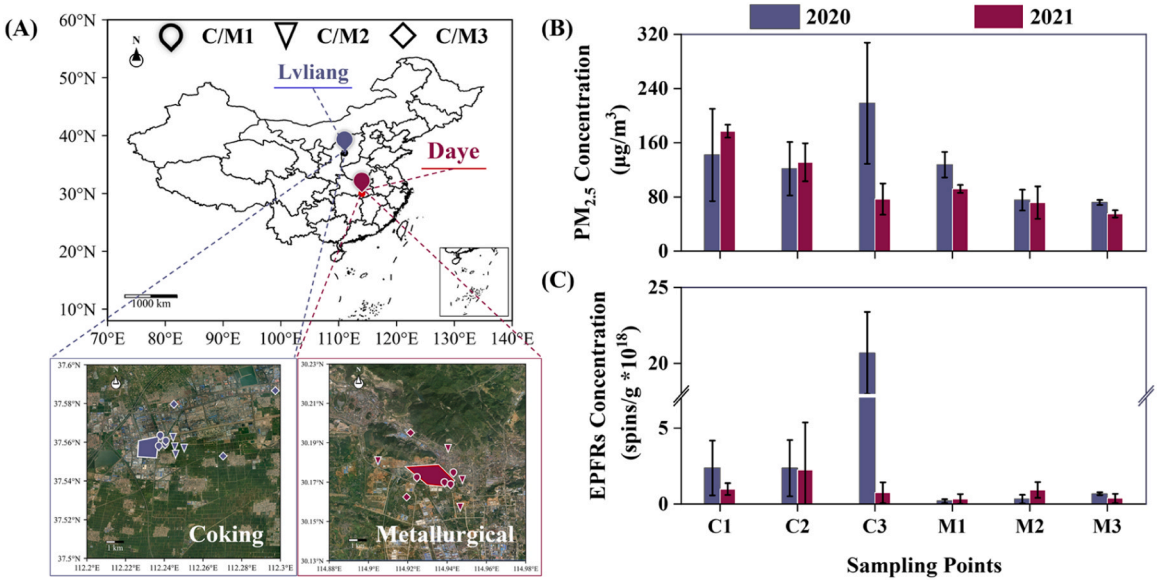

Fig. 1. Overview of sampling sites and pollutant levels. (A) Map of sampling sites categorized as Coking and Metallurgy industry zones. (B) Average $PM_{2.5}$ concentrations across sites. (C) Average EPFR concentrations. (C = Coking, M = Metallurgy; Numerals (1−3) denote buffer distances: < 1 km, 1–2 km, and > 2 km, respectively).

distribution and higher overall g-values, suggesting a significantly higher proportion of oxygen-centered radicals and metal-coordinated radicals [26]. The ΔH_{p-p} parameter, representing the sensitivity of unpaired electrons to their chemical microenvironment, acts as a spectral line width indicator-higher values typically correlate with greater EPFR diversity. The $\Delta H_{p\text{-}p}$ of EPFRs in both these two zones ranged from 3 to 13 G.

Compared to 2020, $PM_{2.5}$ concentrations at C1 and C2 increased by 24.76% and 7.98% in 2021, while C3 decreased significantly by 64.81%. Corresponding EPFR concentrations decreased by 58.40%, 4.66%, and 96.38% at these sites. In contrast, all sites in metallurgical zone showed declining $PM_{2.5}$ concentrations (28.13%, 5.02%, and 23.27% for M1, M2, and M3), but EPFR concentrations exhibited inconsistent trends (68.32% and 180.97% increases at M1 and M2, and 43.95% decrease at M3). Although $PM_{2.5}$ acts as the primary environmental carrier for EPFRs, these completely mismatched interannual variation trends indicate no direct correlation between $PM_{2.5}$ and EPFR concentrations in coking and metallurgical industry zones (coking: $n = 22$, Pearson $r = -0.248$, $p = 0.266$; Spearman $r_s = -0.268$, $p = 0.227$, metallurgy: $n = 20$, Pearson $r = -0.039$, $p = 0.870$; Spearman $r_s = -0.056$, $p = 0.816$). This decoupling phenomenon may be related to exogenous input from mixed atmospheric sources or atmospheric secondary processes [33,44], which will be further verified through principal component analysis of particulate chemical components in the following section.

The decoupling between $PM_{2.5}$ mass concentration and EPFR abundance confirms that total particulate mass is not the dominant factor controlling EPFR formation, whereas the intrinsic chemical composition of $PM_{2.5}$ may infect the industry differences in EPFR characteristics. FTIR characterization results (Figs. S7-S8) showed that the functional groups of $PM_{2.5}$ from both zones were dominated by O-H, aromatic C-H, alkane C-H, C═O, and aromatic C═C. The relative abundances of O-H, aromatic C-H, and alkane C-H were comparable between the two zones, at approximately 40%, 5%, and 7%, respectively, while differences were observed in the relative contents of C═O and aromatic C═C. The C═O content was 16.7% and 4.3% for coking and metallurgical $PM_{2.5}$, respectively, whereas the aromatic C═C content reached 29.2% in coking $PM_{2.5}$ and 39.1% in metallurgical $PM_{2.5}$. Elemental analysis via SEM and EDS (Figs. S9-S13) further validated the distinct compositional profiles of $PM_{2.5}$ from the two zones. Coking $PM_{2.5}$ was dominated by C, O, and Si, accounting for 28.3%, 35.9%, and 26.3% of the total elemental composition, respectively. In contrast, metallurgical $PM_{2.5}$ had a significantly lower carbon content (0.9%) but was highly enriched in O (56.1%) and Si (34.1%), with the total proportion of inorganic mineral elements including Ca, Al, Fe, and Mg exceeding 9% in both zones.

The observed differences in the chemical properties of ambient $PM_{2.5}$ are likely associated with the inherent differences in fuel and production technologies between the two industrial sources. The coking process is dominated by oxygen-deficient pyrolysis of bituminous coal at moderate temperatures [45], where coal matrix decomposition releases large amounts of volatile organic matter and forms carbon-rich fly ash particles. In comparison, the metallurgical process involves high-temperature smelting reduction of anthracite-ore mixtures [46], where the fuel is dominated by high-carbonization anthracite and inorganic ore components, with limited release of organic volatiles during thermal. The compositional differences observed in field samples are fully consistent with these process characteristics. The high carbon content and abundant aromatic carbon groups in coking $PM_{2.5}$ directly corresponded to the pyrolysis of bituminous coal rich in volatile components, while the low carbon content and high inorganic element abundance in metallurgical $PM_{2.5}$ aligned with the ore-mixed smelting fuel system.

From the perspective of fuel chemistry and EPFR formation mechanisms, the bituminous coal used for coking is rich in labile volatile carbon and organic precursors [47,48], which readily undergo pyrolytic cleavage under oxygen-deficient conditions to generate abundant radical intermediates. These intermediates further bind to carbon-rich fly ash carriers to form stable carbon-centered EPFRs, which explains the high EPFR concentrations and low, narrowly distributed g-factors observed in the coking zone. Anthracite used in metallurgical processes in contrast has a dense structure, high carbonization degree and scarce active functional groups [49,50], which results in far fewer radical intermediates generated during thermal treatment and thus lower EPFRs yields. The abundant transition metals including Si and high oxidation degree of organic matter in metallurgical $PM_{2.5}$ promote the formation of oxygen-centered and metal-coordinated radicals [51], which is consistent with the wider g-factor distribution in the metallurgical. The diverse organic precursors in bituminous coal also generate a wider variety of radical species during pyrolysis, which leads to a more complex microchemical environment for unpaired electrons and higher $\Delta H_{p\text{-}p}$ values in coking samples [31].

In summary, significant source-specific differences existed in the concentration, g-factor and $\Delta H_{p\text{-}p}$ of EPFRs surrounding coking and metallurgical industries. The thermal treatment processes and fuel characteristics likely jointly determined the initial formation capacity of EPFRs.

3.2. EPFRs generated from thermal treatment of bituminous coal and anthracite

Given the findings in 3.1 indicating that fuel and thermal treatment conditions may influence the generation of EPFRs, this section presents laboratory-scale thermal simulations of coking bituminous coal and metallurgical anthracite conducted over a temperature range of 200–700 ℃, followed by an evaluation of EPFRs characteristics within the resulting thermal residues (fly ash and coal cinder).

In this study, two types of thermal residues, namely fly ash and coal cinder, were collected from the thermal treatment of bituminous coal and anthracite, respectively. Thermal results showed that anthracite produced negligible fly ash during thermal treatment (Fig. 2**A** and Table S2), which is consistent with its inherent physicochemical properties [52]. Meanwhile, the signals of EPFRs in raw coal, corresponding cinder and fly ash were detected (Fig. 2**B**). The g-factors of bituminous coal and its cinder were 2.0026 and 2.0026, respectively, while those of anthracite and its cinder were 2.0024 and 2.0026, respectively. However, no obvious EPFR signal was detected in the anthracite fly ash, while a strong EPFR signal was observed in bituminous coal fly ash. Further FTIR, SEM and EDS analyses (**Figs. 2C−2D** and **S14-S15**) confirmed a strong correlation in elemental composition (C/O) and organic functional groups (e.g., OH) between the coals, coal cinder, and $PM_{2.5}$. Based on this analysis, coal cinder as the primary solid residue of thermal treatment, effectively links the simulated experiments to field conditions and thus serves as a representative matrix. Consequently, coal cinder was selected as the primary focus for subsequent experiments.

Since incomplete thermal treatment is a prerequisite for EPFR formation [38], this study systematically investigates the effects of key incomplete thermal treatment conditions (time and temperature) on the formation and characteristic evolution of EPFRs. Incomplete thermal treatment stages are widely present in the core process sections of both coking and metallurgical industries (Fig. S1). Time-dependence studies revealed that the EPFR concentration in coal cinder from bituminous coal tended to stabilize after 30 min of thermal treatment under 500 ℃ (Fig. S16), establishing this duration as the standard temperature for subsequent experiments. Temperature-dependence studies demonstrated that within the 200–500 ℃ range (Fig. S17A-S17E), the EPFR concentration in coal cinder continuously increased with rising temperature, reaching a peak at 500 °C (bituminous coal: 50.4×10^{18} spins g^{-1}; anthracite: 72.2×10^{18} spins g^{-1}). The reason why 500 °C is the optimal temperature for EPFR formation is that this temperature range not only provides sufficient thermal energy for the pyrolysis of organic

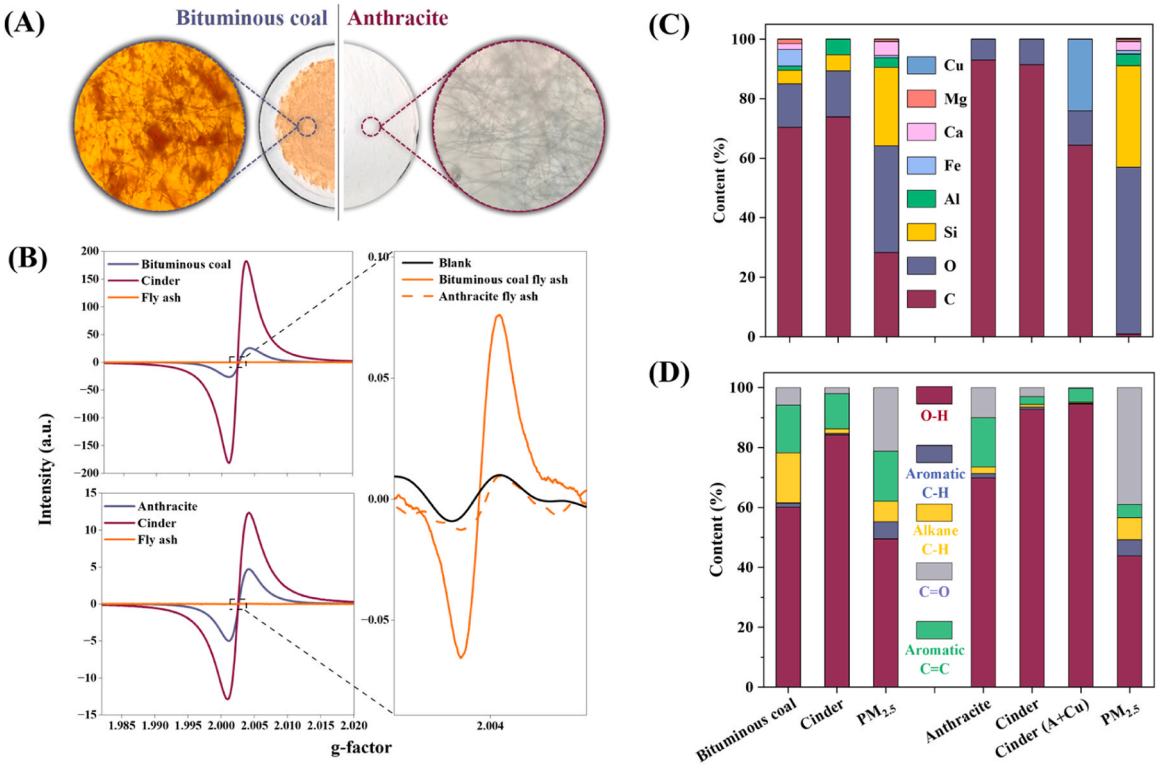

Fig. 2. Characterization of combustion products from bituminous coal and anthracite. (A) Photographic and microscopic morphology of fly ash. The left and right panels show collection filters loaded with fly ash from bituminous coal and anthracite combusted at 500 ℃ for 30 min, respectively. The middle and two circular insets display the visual and microscopic (20 × objective) details of the corresponding fly ash samples. (B) EPR signals are compared between combustion products (cinder, fly ash) of bituminous coal (top panel) and anthracite (bottom panel) at 500 °C. (C) Elemental composition and (D) Functional group of raw coal, cinder (500 ℃), and ambient $PM_{2.5}$. "A + Cu" denotes a mixture of anthracite and basic copper carbonate.

precursors in coal to generate radical intermediates, but also avoids excessive oxidation of intermediates [53]. Meanwhile, the metal oxides in coal are activated at this temperature, which can adsorb and stabilize radical intermediates to form EPFRs [24,54]. However, when the temperature was further increased to 600–700 °C, the EPFR concentration dropped sharply to below the detection limit, which is mainly due to the complete oxidation of organic precursors at high temperatures, the loss of radical generation sources, and the quenching of existing EPFRs caused by intense thermal treatment motion and oxidative reactions at high temperatures [55]. Notably, the g-factor (2.0024–2.0030) and $\Delta H_{p\text{-}p}$ (4–6 G) of the EPFRs remained essentially constant across the entire temperature range, indicating that incomplete thermal treatment temperature primarily affects the generation concentration of EPFRs, rather than g-factor and $\Delta H_{p\text{-}p}$.

To simulate the raw material characteristics of the metallurgical industry, we added 5 wt%, 10 wt%, and 15 wt% basic copper carbonate to anthracite. The results showed that with increasing mineral content (Fig. S17F-S17H), the addition of 15 wt% basic copper carbonate, the EPFR concentration in anthracite cinder decreased by 55% compared with pure anthracite cinder under the same thermal treatment condition, while the g-factor and $\Delta H_{p\text{-}p}$ remained stability. This concentration reduction is primarily attributed to the dilution effect of malachite on the anthracite organic matrix [56], and we cannot rule out the potential quenching effect of copper ions on EPFRs, the copper ions may accept electrons from unpaired electrons of radicals, leading to the disappearance of free radical properties [57].

Laboratory simulation data (Fig. S17C-S17H) showed no significant fluctuation in the g-factor and $\Delta H_{p\text{-}p}$ of EPFRs from bituminous coal, anthracite-Cu mixtures, and their derived cinders. These findings strongly suggest that the thermal treatment process does not significantly alter the g-factor and $\Delta H_{p\text{-}p}$ of the EPFRs. This is supported by Zhang et al., who reported that thermal treatment temperature explained 50% and 19% of the variation in g-factor and $\Delta H_{p\text{-}p}$, respectively, while fuel accounted for 61% of the variation in $\Delta H_{p\text{-}p}$ [31], further supporting the conclusion that fuel characteristics are the key determinants of EPFRs properties such as g-factor and $\Delta H_{p\text{-}p}$. While EPFR concentrations in coal cinders from bituminous coal and anthracite exhibited no order-of-magnitude difference, both significantly exceeded those found in $PM_{2.5}$ from coking and metallurgical industry zones. This discrepancy is likely attributable to differential particle generation capacity during incomplete fuel thermal treatment. As shown in Table S2, thermal treatment of 1.5 g samples at 500 ℃ for 30 min yielded 0.93 g and 1.38 g of cinder from bituminous coal and anthracite, respectively, but produced only 0.0052 g and 0.0008 g of thermal-derived particles. Crucially, bituminous coal demonstrated substantially greater particle generation capacity than anthracite (inherent fuel property). This directly accounts for the higher ambient $PM_{2.5}$ levels and associated EPFR concentrations observed in coking operations compared to metallurgical processes (Fig. 1**B-1C**). Therefore, the capacity of industry-specific fuels to generate particulate matter during thermal treatment governs their atmospheric EPFR emission potential, the actual stack emission factors should be further tested in future on-site measurements.

In summary, fuel not only determined the electronic structure of EPFRs but also, by influencing the form (coal cinder vs. particulate matter) and yield of thermal products, ultimately determined their concentration levels in environmental media.

3.3. Characterization of $PM_{2.5}$ composition and EPFRs based on principal component analysis

In this section, we performed principal component analysis (PCA) on elemental composition, functional groups and EPFR-related parameters of coking and metallurgical samples, combined with laboratory

simulation data to verify the link between fuel composition and EPFR formation and to clarify source-specific pollution traits, component-EPFR correlations and interannual variations of $PM_{2.5}$-bound EPFRs.

For coking field samples (Fig. 3**A**), PC1 and PC2 explained 31.2% and 21.3% of total variance respectively, with clear separation between 2020 and 2021 samples, indicating significant interannual shifts in $PM_{2.5}$ compositional characteristics. The 2020 samples distributed in the positive PC1 direction, overlapping with loadings of total carbon (C), aromatic C═C/C-H, alkane C-H, Fe, Mg and $PM_{2.5}$, reflecting a pollution profile dominated by primary carbonaceous and metal-bearing particles from coal pyrolysis and incomplete combustion. The 2021 samples clustered in the negative PC1 and positive PC2 direction, consistent with loadings of oxygen (O), C═O group, Ca, Si and $\Delta H_{p\text{-}p}$, indicating enhanced particulate oxidation and secondary transformation. This result directly explained the interannual variation phenomenon observed in 3.1 that $PM_{2.5}$ concentration increased but EPFR concentration decreased in the coking industry zone in 2021. The increased proportion of secondary oxidation components and exogenous dust components in 2021 samples exerted a dilution effect on EPFRs enriched from primary combustion sources. This dilution effect of combustion source particles on ambient EPFRs has been widely reported in previous field studies on industrial and urban atmospheric EPFRs [58].

The loading arrows of EPFRs and g-factor were nearly collinear, showing a significant positive correlation with C, and a negative correlation with O, C═O group, Ca and Si. This indicated that EPFRs in the coking samples were dominated by the carbon-centered environment. The $\Delta H_{p\text{-}p}$ was significantly positively correlated with O, and negatively correlated with C, indicating that the variation of radical line width was mainly affected by the oxidation degree of particulate matter and inorganic mineral components. This phenomenon can be ascribed to the accelerated spin-lattice relaxation rates induced by paramagnetic oxygen species adsorbed onto carbon surfaces [59]. Most importantly, the PCA results of coking field samples were highly consistent with the component characteristics of laboratory bituminous coal cinder (Fig. 2**C**−**2D**), indicating that chemical components in coking derived coal cinder had a direct relationship with PCA results of coking field samples. This study is highly consistent with the classic formation mechanism of carbon-centered EPFRs from coal pyrolysis reported in previous studies [60,61].

For metallurgical field samples (Fig. 3**B**), PC1 and PC2 accounted for 31.4% and 14.8% of total variance respectively, also showing distinct interannual differentiation. The 2020 samples distributed in positive PC1, close to loadings of organic carbon functional groups, Fe, Mg and $PM_{2.5}$, reflecting primary organic-metal composite emissions. The 2021 samples shifted to the negative PC2 direction, overlapping with EPFRs, Si, $\Delta H_{p\text{-}p}$ and g-factor loadings, and approaching Fe, Mg, O and C═O loadings, indicating EPFR evolution was closely linked to metal-catalyzed oxidation and Si-containing minerals. This is consistent with the formation mechanism of metal-assisted radical generation in high-temperature metallurgical processes [38,62]. Unlike coking samples, the EPFRs and g-factor in metallurgical samples were positively correlated with Si and $\Delta H_{p\text{-}p}$ but negatively correlated with Ca, with no primary dependence on carbonaceous matrices. The g-factor was collinear with EPFRs and metal/oxidative components, indicating dominant oxygen-centered or metal-associated radicals, distinct from coking's carbon-centered radicals. This finding aligns with previous studies demonstrating that mineral surfaces can stabilize transition metal ions and promote radical formation through surface-mediated electron transfer reactions [37]. In sharp contrast to the coking samples, the PCA results of metallurgical field samples had no obvious correspondence with the component characteristics of laboratory anthracite coal cinder (Fig. 2**C**−**2D**), meaning that the opposite was true for metallurgical samples. This confirmed that the inherent property of anthracite with extremely low particulate matter generation capacity (Table S2). The poor correspondence between PCA results and coal cinder also indicates that single coal combustion simulation cannot effectively reproduce the actual EPFR characteristics of metallurgical industry zone.

The commonality was that EPFRs had no significant linear correlation with $PM_{2.5}$ concentration in both industry zones ($PM_{2.5}$ and EPFRs loadings were nearly perpendicular), indicating that the specific chemical composition of $PM_{2.5}$, rather than total mass, dominated the formation and stabilization of EPFRs. The result is consistent with the results of multi region field studies on atmospheric EPFRs in China [58]. This finding confirms that $PM_{2.5}$ concentration is not a valid proxy for EPFR pollution and health risk assessment. Both industry zones showed identical interannual trends, with primary emission dominance in 2020 and significantly enhanced oxidation and secondary transformation in 2021. This reflected that under the background of strengthened regional air pollution control, primary particulate matter emissions have been controlled to a certain extent, while the impacts of gas-phase and particle-phase oxidation processes as well as secondary transformation on the formation and evolution of EPFRs have become increasingly prominent. This interannual variation trend is in excellent agreement with previously documented evolution patterns of atmospheric particulate components under the implementation of China's Clean Air Actions [63,64]. Against this background, the secondary transformation of EPFRs should also receive sufficient attention [65]. The core difference was that coking source EPFRs were carbon-centered radicals generated from bituminous coal pyrolysis, highly coupled with carbonaceous components, while metallurgical source EPFRs were oxygen-centered or metal-associated radicals regulated by transition metals, silicon-containing minerals and secondary oxidation processes, with weak dependence on coal-derived carbonaceous particles.

In summary, PCA analysis verified the intrinsic differences in origin

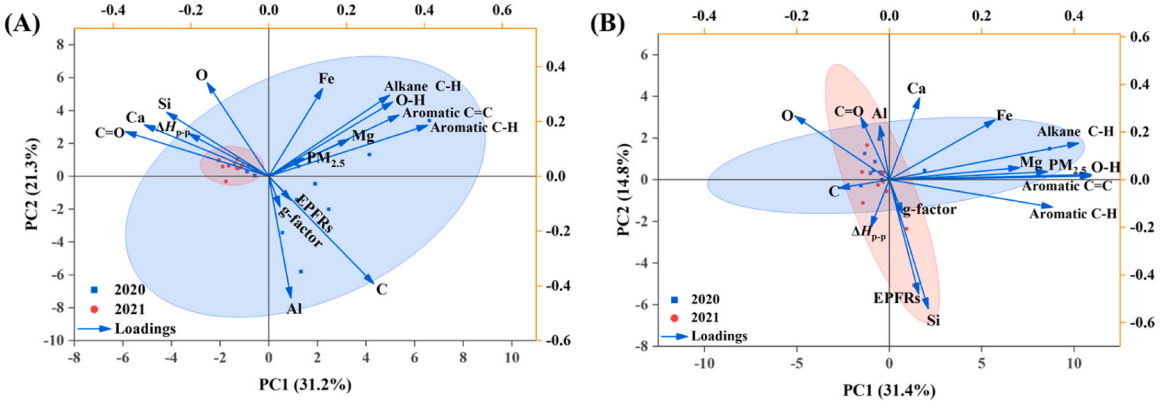

Fig. 3. PCA between EPFRs and functional groups/elements. (A) coking industry, (B) metallurgical industry. The sample colors distinguish years (blue for 2020, red for 2021), and blue arrows indicate the direction and strength of variable loadings.

and formation mechanism of EPFRs between coking and metallurgical industry zones from a multivariate statistical perspective. It further confirmed the decisive role of fuel on the core characteristics of EPFRs, and identified g-factor and $\Delta H_{p\text{-}p}$ as stable source-specific fingerprints of industrial EPFRs.

3.4. Environmental risks of $PM_{2.5}$-bound EPFRs from coking and metallurgical industry zones

Through cross-validation between field monitoring and laboratory simulation, this study identified the core mechanisms driving divergent emission characteristics of EPFRs from coking and metallurgical industry zones (Fig. 4**A**). The concentration of EPFRs in $PM_{2.5}$ around coking industry zone was approximately one order of magnitude higher than that around metallurgical industry zone, a discrepancy driven not by intrinsic differences in EPFR formation potential between the two industries, but directly by the gap in particulate matter generation capacity of their respective fuels. Laboratory simulation confirmed that both bituminous coal and anthracite generated high levels of EPFRs on the order of 10^{19} spins g^{-1} under incomplete thermal treatment at 500 ℃. However, the dense carbonaceous structure of anthracite yielded extremely low fly ash output, with the vast majority of generated EPFRs sequestered in coal cinder, resulting in negligible direct atmospheric emissions to surrounding areas. This finding revealed that even within coal-fueled industrial sectors, emerging pollutants presented fundamentally distinct emission profiles and environmental fates. Specifically, as a high-intensity source of atmospheric EPFRs, the coking industry should prioritize source reduction of EPFR precursors during thermal treatment and in-process control of fly ash emissions. In contrast, while the metallurgical industry had minimal direct atmospheric EPFR emissions, its coal cinder harbored EPFRs at concentrations comparable to those from coking operations. Fly ash emission via stacks is the dominant primary pathway for atmospheric EPFRs from the coking industry, and the fugitive cinder dust is a non-negligible secondary pathway, especially for the metallurgical industry where cinder output is large, requiring targeted oversight of multi-media environmental release risks of this solid waste throughout its full lifecycle. These EPFRs can be released into the atmosphere via fugitive dust resuspension during stockpiling and transportation, leach into soil and groundwater via rainwater eluviation, and pose direct exposure risks during landfill disposal and resource recovery processes. A growing body of existing research also contended that it was inappropriate to treat all thermal treatment sources as a single homogeneous entity, and that more refined differentiation was warranted in source apportionment, risk assessment and regulatory oversight [30,32,66].

The distinct sector-specific emission profiles of EPFRs further raised the demand for reliable tracers to support accurate source identification of atmospheric EPFRs. While particulate matter acted as the primary carrier for EPFRs to enter the atmosphere [66], field monitoring data within a 2 km radius of facilities in both sectors consistently showed no significant linear correlation between ambient $PM_{2.5}$ mass concentrations and EPFR abundances. This decoupling effect invalidated the use of $PM_{2.5}$ mass concentration as a proxy indicator for atmospheric EPFR pollution levels and associated health risks. In comparison, this study confirmed that the g-factor and $\Delta H_{p\text{-}p}$, which were inherently determined by the intrinsic chemical properties of fuels, should serve as robust and stable tracers for atmospheric EPFR source identification. Even within coal-fueled industrial sectors, coking and metallurgical industries presented clearly distinguishable, sector-specific signatured in EPFR g-factor and $\Delta H_{p\text{-}p}$ (Fig. 4**B**). Meanwhile, these two core structural parameters were solely governed by inherent fuel, while incomplete thermal treatment processing temperature and light irradiation (365 nm ultraviolet photolysis conditions) (Fig. S18) only induced fluctuations in EPFR concentrations without altering their intrinsic structural characteristics. This finding not only underscored the critical need for systematic, sector-specific characterization of industrial EPFR emission profiles, but also provided a solid methodological basis for quantitative source apportionment and pollution tracing of atmospheric EPFRs. The real atmospheric aging involves complex heterogeneous oxidation by O_3, ·OH and NO_3·, as well as effects of humidity and secondary organic aerosol coating, which may have more complex impacts on EPFR evolution. Multi-factor simulated aging experiments are an important direction for future research.

The decoupling phenomenon between ambient $PM_{2.5}$ mass

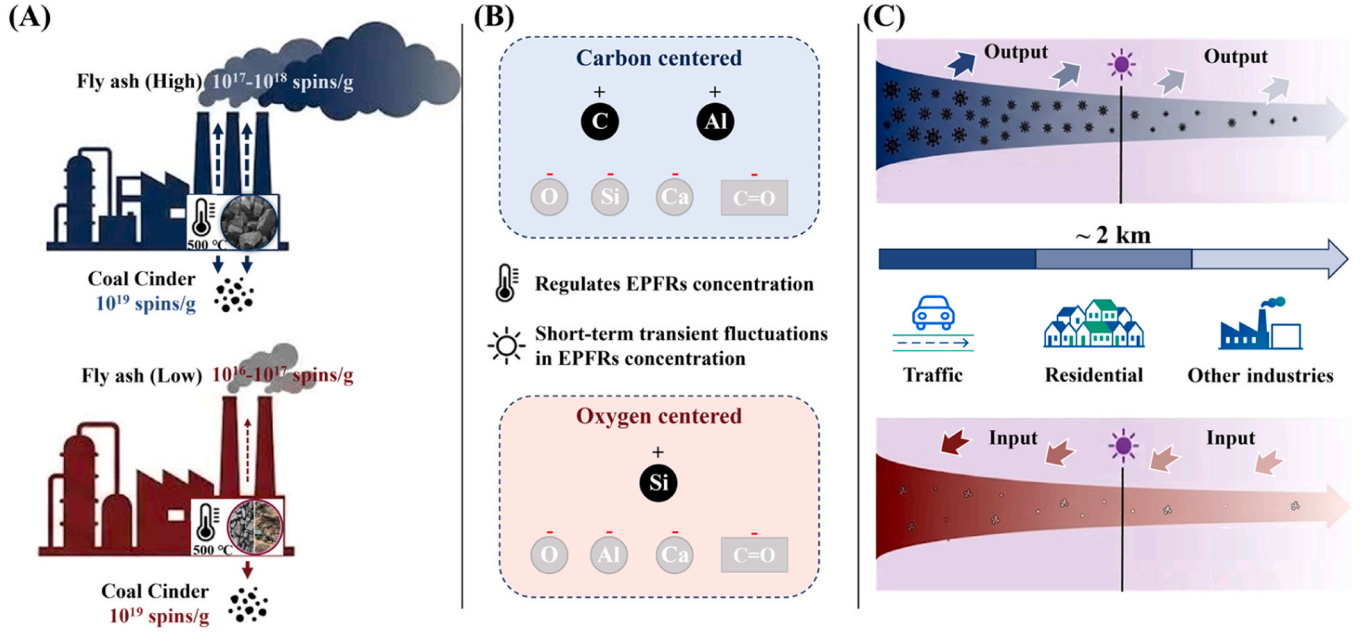

Fig. 4. Release pathways, diagnostic markers, and environmental contributions of EPFRs from coking and metallurgical thermal treatment processes. (A) Concentrations of EPFRs in cinder and fly ash. (B) Identification of characteristic factors for source apportionment. The g-factors distinguish carbon-centered radicals (coking) from oxygen-centered radicals (metallurgy). (C) Conceptual model of EPFRs within ~2 km of the source. The schematic illustrates the output from coking and input from metallurgy, integrated with contributions from traffic, residential, and other industrial sources.

concentrations and $PM_{2.5}$-bound EPFRs abundances observed in the two industrial in this study is closely associated with exogenous inputs from mixed atmospheric sources and atmospheric secondary transformation processes [67,68]. For the coking industry zone, the consistent detection of high EPFRs concentrations across all sampling sites and monitoring years confirmed that it acted as a stable and dominant emission source of atmospheric EPFRs in the surrounding ambient air. Relevant studies have verified that EPFR concentrations in ambient air surrounding coking plants were 1–2 orders of magnitude higher than those in urban background sites, identifying coking operations as one of the key contributors to atmospheric EPFRs within coal-fueled industrial sectors [60]. For the metallurgical industry zone, the vast majority of EPFRs generated during production processes were sequestered in coal cinder, with an extremely low proportion of EPFRs directly emitted to the atmospheric environment via flue gas. This limited direct emission meant that metallurgical operations did not dominate the EPFR concentration levels in the surrounding ambient air. Existing source apportionment studies have reported that non-industrial combustion sources including vehicle traffic, residential coal combustion, and other scattered industrial [58,59,69] emissions collectively exogenous EPFR from long-range regional atmospheric transport [16] also exerted a significant superimposed effect on ambient EPFR concentration levels. The observational results of this study further confirmed that exogenous input was the core factor driving the variation of EPFR concentrations in the metallurgical, as dense roads, industrial facilities, and residential areas were distributed around both coking and metallurgical industries (Fig. S19). This stark contrast in source contribution patterns between the two industries further confirmed that the coking industry served as a stable endogenous emission source of EPFRs to the surrounding atmospheric environment. Based on current evidence including the negligible fly ash formation potential of anthracite and the mismatch between field samples and lab cinder in PCA, we infer that exogenous input from regional mixed sources is an important driver of EPFR levels in the metallurgical zone (Fig. 4**C**). However, quantitative source apportionment models (e.g., Positive Matrix Factorization, Chemical Mass Balance) and air mass trajectory analysis (e.g., Hybrid Single-Particle Lagrangian Integrated Trajectory) were not applied in this study. Therefore, the inference regarding exogenous EPFR input remains tentative and requires further validation in future work using more comprehensive source apportionment approaches.

4. Conclusions

This study systematically elucidated the emission characteristics and regulatory mechanisms of $PM_{2.5}$-bound EPFRs from coking and metallurgical industry zones via 2020–2021 field observations and laboratory simulations. The 10-fold higher EPFR levels in coking zones are attributed to bituminous coal labile organic precursors and higher fly ash yield compared to anthracite. We demonstrate that fuel properties dictate the structural traits (g-factor, $\Delta H_{p\text{-}p}$) of EPFRs, while thermal treatment conditions govern formation efficiency, with light merely inducing transient concentration fluctuations. PCA analysis further supported this conclusion, which the g-factors of coking EPFRs positively correlated with C, but negatively with O, C═O, Ca, and Si, while $\Delta H_{p\text{-}p}$ showed the opposite trend. The metallurgical EPFRs g-factor positively correlated with Si, but negatively with O, C═O, and Al, while $\Delta H_{p\text{-}p}$ negatively correlated with Ca. Critically, we identify coking industries as direct sources exporting EPFRs to the surrounding environment, whereas metallurgical zone are influenced by exogenous mixing, while the elevated EPFR concentrations retained in coal cinder from both industries warrant significant attention. This study has non-negligible limitations including limited universal applicability from only covering two typical coal based heavy industries, the lack of synchronous site-specific meteorological data and field sampling replicates can lead to uncertainty in absolute concentration measurements, a small sample size may not be able to reliably detect weak correlations, and insufficient environmental factor selection in photochemical aging experiments. Overall, this work provides a solid scientific basis for source specific health risk assessment and precise emission control of industrial radicals, and future research will expand to more coal based industrial sectors.

Environmental Implication

This study reveals that fuel governs EPFR emissions from coking and metallurgical industry zones, with critical implications for revising current air pollution control frameworks. It confirms a complete decoupling between $PM_{2.5}$ and EPFR concentrations, indicating that reducing $PM_{2.5}$ alone cannot effectively mitigate the oxidative stress and respiratory health risks posed by EPFRs. The identified source-specific g-factor and $\Delta H_{p\text{-}p}$ serve as reliable tracers for accurate atmospheric EPFR source apportionment. The coking industry is a high-intensity stable EPFR source, with fly ash emissions from bituminous coal pyrolysis requiring priority control. Risks from the metallurgical industry lie in full-lifecycle multi-media release of coal cinder. Notably, metallurgical zone act as exogenous EPFR receptors, highlighting the need for regional coordinated control.

Significance of This Work

Coal-based industrial thermal processes remain the dominant anthropogenic source of atmospheric fine particulate matter and associated emerging pollutants, including environmentally persistent free radicals (EPFRs). These radical species exhibit long environmental persistence and strong oxidative toxicity, posing non-negligible risks to atmospheric environmental quality and public health, and have become a key focus of atmospheric chemistry and pollution control research in recent years. While stringent clean air regulations have achieved substantial reductions in conventional primary pollutants from coal-fueled industrial sectors, systematic understanding of the emission characteristics, driving mechanisms and environmental behaviors of EPFRs from typical coal-based heavy industries remains limited. In particular, few studies have conducted synchronous comparative analysis of EPFRs between pure coal pyrolysis systems represented by coking and coal-ore mixed combustion systems represented by metallurgy. This critical knowledge gap has hindered the accurate source apportionment of atmospheric EPFRs and the development of source-specific pollution control strategies.

Our work addressed this gap by integrating field observations in typical coking and metallurgical industry zones, laboratory-scale thermal simulation experiments across a temperature gradient of 200–700 ℃, and photochemical aging experiments under controlled light intensities, to systematically characterize the key parameters of EPFRs and the physicochemical properties of their carrier particulate matter. Cross-validation between field monitoring and laboratory simulation revealed that the concentration of EPFRs in ambient air around the coking zone was an order of magnitude higher than that around the metallurgical zone. This discrepancy was not driven by intrinsic differences in EPFRs formation potential between the two fuel types, but directly by the 6.5-fold gap in fly ash yield between bituminous coal and anthracite during thermal processing. We further confirmed that the inherent properties of the fuel were the sole determinant of the core structural parameters of EPFRs, the g-factor and $\Delta H_{p\text{-}p}$, while thermal processing temperature and light irradiation only induced short-term fluctuations in radical concentration without altering their intrinsic structural characteristics. This result provides a stable and reliable tracer for accurate source identification of atmospheric EPFRs. Consistent field data from both industrial zones show no significant correlation between $PM_{2.5}$ mass concentration and EPFRs abundance, indicating that the chemical composition of particulate matter, rather than total mass, dominates the formation and stabilization of these radicals.

This information should be of high interest to researchers in the

fields of Environmental Science and Engineering on Hazardous Materials. Of course, these results are also of significant interest to the reader of "***Journal of Hazardous Materials***".

CRediT authorship contribution statement

Xiaoyao Ma: Data curation. **Jiangyao Chen:** Writing – review & editing, Supervision, Conceptualization. **Shunyu Ding:** Investigation, Data curation. **Chenxu Gao:** Writing – original draft, Methodology, Investigation, Formal analysis.

Supporting Information

The Supporting Information is available free of charge on the website, including additional information on the experimental methods and supporting data.

Declaration of Competing Interest

The authors declare that they have no known competing financial interests or personal relationships that could have appeared to influence the work reported in this paper.

Acknowledgments

This work was financially supported by the National Natural Science Foundation of China (42577424), National Key Research & Development Program of China (2019YFC1804500) and Guangzhou Basic and Applied Basic Research Scheme (2024A04J6358).

Appendix A. Supporting information

Supplementary data associated with this article can be found in the online version at doi:10.1016/j.jhazmat.2026.142964.

Data availability

Data will be made available on request.

References

[1] Steven, Chu, Arun, Majumdar, 2012. Opportunities and challenges for a sustainable energy future. Nature 488, 294–303.
[2] Wang, X.L., Lu, C., Shi, B.F., Chen, Y., Han, Z.X., Nathwani, J., 2024. Decomposition analysis, decoupling status, and future trends of energy consumption in China's iron and steel industry. Environ Dev Sustain 26, 885–908.
[3] Agency, I.E., 2024. Coal 2024: Analysis and Forecast to 2027. IEA, Paris.
[4] Yang, S.M., Zhang, G.R., 2012. Study on technologies and countermeasures of comprehensive utilization of coal resources. Trans Tech Publ Ltd 3001–3004.
[5] Krzesinska, M., Szeluga, U., Smedowski, L., Majewska, J., Pusz, S., Czajkowska, S., Kwiecinska, B., 2010. TGA and DMA studies of blends from very good coking Zofiowka coal and various carbon additives: Weakly coking coals, industrial coke and carbonized plants. Int J Coal Geol 81, 293–300.
[6] H. Schmitt, M. Chouaib, Increasing the strength of blast-furnace coke - by adding specified metal or oxide to coking coal, in, Still Fa Carl (Silc-C).
[7] Speight, J., 2015. Handb COAL Anal.
[8] Klimont, Z., Kupiainen, K., Heyes, C., Purohit, P., Cofala, J., Rafaj, P., Borken-Kleefeld, J., Schöpp, W., 2017. Global anthropogenic emissions of particulate matter including black carbon. Atmos Chem Phys 17, 8681–8723.
[9] Shen, H.Z., Huang, Y., Wang, R., Zhu, D., Li, W., Shen, G.F., Wang, B., Zhang, Y.Y., Chen, Y.C., Lu, Y., Chen, H., Li, T.C., Sun, K., Li, B.G., Liu, W.X., Liu, J.F., Tao, S., 2013. Global Atmospheric Emissions of Polycyclic Aromatic Hydrocarbons from 1960 to 2008 and Future Predictions. Environ Sci Technol 47, 6415–6424.
[10] Pacyna, E.G., Pacyna, J.M., Sundseth, K., Munthe, J., Kindbom, K., Wilson, S., Steenhuisen, F., Maxson, P., 2010. Global emission of mercury to the atmosphere from anthropogenic sources in 2005 and projections to 2020. Atmos Environ 44, 2487–2499.
[11] Liu, H.M., Lei, J., Liu, Y.W., Zhu, T., Chan, K.H., Chen, X., Wei, J., Deng, F.R., Li, G., Jiang, Y.X., Bai, L.J., Wang, K., Chen, J., Lan, Y., Xia, X., Wang, J.X., Wei, C., Li, Y.X., Chen, R.J., Gong, J.C., Duan, X.L., Zhang, K., Kan, H.D., Shi, X.M., Guo, X. B., Wu, S.W., 2025. Hospital admissions attributable to reduced air pollution due to clean-air policies in China. Nat Med 31, 1688–1697.
[12] Zheng, B., Tong, D., Li, M., Liu, F., Hong, C.P., Geng, G.N., Li, H.Y., Li, X., Peng, L. Q., Qi, J., Yan, L., Zhang, Y.X., Zhao, H.Y., Zheng, Y.X., He, K.B., Zhang, Q., 2018. Trends in China's anthropogenic emissions since 2010 as the consequence of clean air actions. Atmos Chem Phys 18, 14095–14111.
[13] Liu, F., Zhang, Q., Ronald, J.V., Zheng, B., Tong, D., Yan, L., Zheng, Y.X., He, K.B., 2016. Recent reduction in NO_x emissions over China: synthesis of satellite observations and emission inventories. Environ Res Lett 11, 114002.
[14] Xu, Y.L., Lu, X.F., Su, G.J., Chen, X., Meng, J., Li, Q.Q., Wang, C.X., Shi, B., 2023. Scientific and regulatory challenges of environmentally persistent free radicals: From formation theory to risk prevention strategies. J Hazard Mater 456, 131674.
[15] Gehling, W., Dellinger, B., 2013. Environmentally persistent free radicals and their lifetimes in $PM_{2.5}$. Environ Sci Technol 47, 8172–8178.
[16] Wei, F.Y., Wang, S.T., Guo, Y.H., Lin, L.X., Xu, T.T., Guo, H.B., 2025. Source apportionment of environmentally persistent free radicals in size-resolved PM: Implications for driving oxidative potential and reactive oxygen species generation. J Hazard Mater 499, 140163.
[17] Khachatryan, L., Vejerano, E., Lomnicki, S., Dellinger, B., 2011. Environmentally persistent free radicals (EPFRs). 1. Generation of reactive oxygen species in aqueous solutions. Environ Sci Technol 45, 8559–8566.
[18] Khachatryan, L., Dellinger, B., 2011. Environmentally Persistent Free Radicals (EPFRs)-2. Are free hydroxyl radicals generated in aqueous solutions? Environ Sci Technol 45, 9232–9239.
[19] Vejerano, E.P., Rao, G.Y., Khachatryan, L., Cormier, S.A., Lomnicki, S., 2018. Environmentally Persistent Free Radicals: Insights on a New Class of Pollutants. Environ Sci Technol 52, 2468–2481.
[20] Zhao, J.F., Shen, G.F., Shi, L., Li, H., Lang, D., Zhang, L., Pan, B., Tao, S., 2022. Real-World Emission Characteristics of Environmentally Persistent Free Radicals in $PM_{2.5}$ from Residential Solid Fuel Combustion. Environ Sci Technol 56, 3997–4004.
[21] Ruan, X.X., Sun, Y.Q., Du, W.M., Tang, Y.Y., Liu, Q., Zhang, Z.Y., Doherty, W., Frost, R.L., Qian, G.R., Tsang, D.C.W., 2019. Formation, characteristics, and applications of environmentally persistent free radicals in biochars: A review. Bioresour Technol 281, 457–468.
[22] Yang, X., Yang, F., Pang, Y.L., Du, C.Y., Wang, K., He, C., Tong, H.J., Liu, F.B., 2025. A critical review of secondary environmentally persistent free radicals: formation, properties, environmental and health impacts. J Hazard Mater 498, 139680.
[23] Feld-Cook, E.E., Bovenkamp-Langlois, L., Lomnicki, S.M., 2017. Effect of Particulate Matter Mineral Composition on Environmentally Persistent Free Radical (EPFR) Formation. Environ Sci Technol 51, 10396–10402.
[24] Liu, S.T., Liu, G.R., Yang, L.L., Li, D., Zheng, M.H., 2022. Critical influences of metal compounds on the formation and stabilization of environmentally persistent free radicals. Chem Eng J 427, 131666.
[25] Chen, Q.C., Sun, H.Y., Wang, M.M., Mu, Z., Wang, Y.Q., Li, Y.G., Wang, Y.S., Zhang, L.X., Zhang, Z.M., 2018. Dominant Fraction of EPFRs from Nonsolvent-Extractable Organic Matter in Fine Particulates over Xi'an, China. Environ Sci Technol 52, 9646–9655.
[26] Dellinger, B., Loninicki, S., Khachatryan, L., Maskos, Z., Hall, R.W., Adounkpe, J., McFerrin, C., Truong, H., 2007. Formation and stabilization of persistent free radicals. Proc Combust Inst 31, 521–528.
[27] Pan, B., Li, H., Lang, D., Xing, B.S., 2019. Environmentally persistent free radicals: Occurrence, formation mechanisms and implications. Environ Pollut 248, 320–331.
[28] Shah, S., Chen, J., Saleem, A.R., Sun, Y.W., Ai, J., Huang, H.Y., Zhang, L.Y., Khan, C., 2025. Source-oriented pollution characteristics and decay kinetics of environmentally persistent free radicals in $PM_{2.5}$ and PM_{10}. J Hazard Mater 495, 139074.
[29] Qian, Z., Chen, Y.J., Liu, Z.Y., Han, Y., Zhang, Y.S., Feng, Y.L., Shang, Y., Guo, H., Li, Q., Shen, G.F., Chen, J.M., Tao, S., 2021. Intermediate Volatile Organic Compound Emissions from Residential Solid Fuel Combustion Based on Field Measurements in Rural China. Environ Sci Technol 55, 5689–5700.
[30] Tian, L.W., Koshland, C.P., Yano, J.K., Yachandra, V.K., Yu, I.T.S., Lee, S.C., Lucas, D., 2009. Carbon-Centered Free Radicals in Particulate Matter Emissions from Wood and Coal Combustion. Energy Fuels 23, 2523–2526.
[31] Zhang, Y.Q., Huang, W.X., Wang, H.C., Huang, T.Y., Luo, Z.H., Li, S.Y., Liu, X.L., Xiao, K., Chen, Q.C., Tao, S., Shen, G.F., 2025. Environmentally Persistent Free Radical Emissions from Indoor Burning of Pelletized Biofuels. Environ Sci Technol 59, 5661–5671.
[32] Wang, P., Pan, B., Li, H., Huang, Y., Dong, X.D., Ai, F., Liu, L.Y., Wu, M., Xing, B.S., 2018. The Overlooked Occurrence of Environmentally Persistent Free Radicals in an Area with Low-Rank Coal Burning, Xuanwei, China. Environ Sci Technol 52, 1054–1061.
[33] Cheng, A.Y., Li, Y., Wu, D., Guo, Z.H., Su, Y., Ding, X., Chen, X., Shao, Y.K., Chen, Q.C., Song, W.H., Ye, X.N., Chen, J.M., Li, Q., 2024. Incomplete solid fuel burning as the major emission source of atmospheric phenols and environmentally persistent free radicals. Fuel 369, 131735.
[34] Yakovleva, E.V., Gabov, D.N., Beznosikov, V.A., Kondratenok, B.M., 2016. Accumulation of polycyclic aromatic hydrocarbons in soils and plants of the tundra zone under the impact of coal-mining industry. Eurasia Soil Sci 49, 1319–1328.
[35] Liu, J.X., Jiang, X.M., Shen, J., Zhang, H., 2015. Influences of particle size, ultraviolet irradiation and pyrolysis temperature on stable free radicals in coal. Powder Technol 272, 64–74.
[36] Trubetskaya, A., Jensen, P.A., Jensen, A.D., Glarborg, P., Larsen, F.H., Andersen, M.L., 2016. Characterization of free radicals by electron spin resonance spectroscopy in biochars from pyrolysis at high heating rates and at high temperatures. Biomass– Bioenerg 94, 117–129.

[37] Jia, H.Z., Zhao, S., Shi, Y.F., Zhu, K.C., Gao, P., Zhu, L.Y., 2019. Mechanisms for light-driven evolution of environmentally persistent free radicals and photolytic degradation of PAHs on Fe(III)-montmorillonite surface. J Hazard Mater 362, 92–98.
[38] Lomnicki, S., Truong, H., Vejerano, E., Dellinger, B., 2008. Copper oxide-based model of persistent free radical formation on combustion-derived particulate matter. Environ Sci Technol 42, 4982–4988.
[39] Aurell, J., Gullett, B.K., Tabor, D., Williams, R.K., Mitchell, W., Kemme, M.R., 2015. Aerostat-based sampling of emissions from open burning and open detonation of military ordnance. J Hazard Mater 284, 108–120.
[40] Xu, M., Wu, T., Tang, Y.-T., Chen, T., Khachatryan, L., Iyer, P.R., Guo, D., Chen, A., Lyu, M., Li, J., Liu, J., Li, D., Zuo, Y., Zhang, S., Wang, Y., Meng, Y., Qi, F., 2019. Environmentally persistent free radicals in PM2.5: a review. Waste Dispos & Sustain Energy 1, 177–197.
[41] Weitkamp, E.A., Lipsky, E.M., Pancras, P.J., Ondov, J.M., Polidori, A., Turpin, B.J., Robinson, A.L., 2005. Fine particle emission profile for a large coke production facility based on highly time-resolved fence line measurements. Atmos Environ 39, 6719–6733.
[42] Liu, S., Kawamura, K., Kunwar, B., Pokhrel, A., Zhan, C.L., Liu, H.X., Zhang, J.Q., Quan, J.H., 2025. Comparing aerosol sources in a metallurgy city: Evidence from low molecular weight organic acids in $PM_{2.5}$ between 2012-2013 and 2021-2022. Urban CLim 59, 102279.
[43] Chen, Q.C., Sun, H.Y., Song, W.H., Cao, F., Tian, C.G., Zhang, Y.L., 2020. Size-resolved exposure risk of persistent free radicals (PFRs) in atmospheric aerosols and their potential sources. Atmos Chem Phys 20, 14407–14417.
[44] Edwards, K.C., Kapur, S., Fang, T., Cesler-Maloney, M., Yang, Y.H., Holen, A.L., Wu, J., Robinson, E.S., DeCarlo, P.F., Pratt, K.A., Weber, R.J., Simpson, W.R., Shiraiwa, M., 2024. Residential Wood Burning and Vehicle Emissions as Major Sources of Environmentally Persistent Free Radicals in Fairbanks, Alaska. Environ Sci Technol 58, 14293–14305.
[45] Shozo, I., Izumi, S., Kiyoshi, F., Hidenori, S., Hirofumi, T., 2008. Prod Metall COKE 2008, 316–324.
[46] Seetharaman, S., Mclean, A., Guthrie, R., Sridhar, S., 2014. Treatise Process Metall.
[47] Dehghani, F., Omidi, F., Heravizadeh, O., Chamgordani, S.B., Gharibi, V., Manesh, A.S., 2020. Occupational health risk assessment of volatile organic compounds emitted from the coke production unit of a steel plant. Int J Occup Saf Ergon 26, 227–232.
[48] Wang, C.Y., Xing, Y.W., Shi, K.Y., Wang, S.W., Xia, Y.C., Li, J.H., Gui, X.H., 2023. Chemical Structure Characteristics and Model Construction of Coal with Three Kinds of Coalification Degrees. ACS Omega 9, 1881–1893.
[49] Seow, W.J., Hu, W., Vermeulen, R., Hosgood, H.D., Downward, G.S., Chapman, R. S., He, X.Z., Bassig, B.A., Kim, C., Wen, C.J., Rothman, N., Lan, Q., 2014. Household air pollution and lung cancer in China: a review of studies in Xuanwei. Chin J Cancer 33, 471–475.
[50] Saik, P., Sybir, A., Vorona, I., Isaieva, O., Yukhymchuk, V., Trachevsky, V., Burchak, O., Hubynskyi, I., Lozynskyi, V., 2025. Research on high-temperature graphitization of anthracite using Raman and electron paramagnetic resonance spectroscopy. Front Earth Sci 13, 1540335.
[51] Jia, H.Z., Nulaji, G., Gao, H.W., Wang, F., Zhu, Y.Q., Wang, C.Y., 2016. Formation and Stabilization of Environmentally Persistent Free Radicals Induced by the Interaction of Anthracene with Fe(III)-Modified Clays. Environ Sci Technol 50, 6310–6319.
[52] Huang, D.B., Chuan, X.Y., Cao, X., 2016. Spectroscopy Characterization of Anthracite Oxide. Spectrosc Spectr Anal 36, 3698–3703.
[53] Yuan, Z.H., Huang, Q.J., Wang, Z.Q., Wang, H., Luo, J.M., Zhu, N.W., Cao, X.D., Lou, Z.Y., 2022. Medium-Low Temperature Conditions Induce the Formation of Environmentally Persistent Free Radicals in Microplastics with Conjugated Aromatic-Ring Structures during Sewage Sludge Pyrolysis. Environ Sci Technol 56, 16209–16220.
[54] Truong H. 2007. Copper(II) oxide mediated formation and stabilization of combustion generated persistent free radicals, 2007.
[55] Wang, Y., Gu, X.F., Huang, Y., Ding, Z.H., Chen, Y.J., Hu, X., 2022. Insight into biomass feedstock on formation of biochar-bound environmentally persistent free radicals under different pyrolysis temperatures. RSC Adv 12, 19318–19326.
[56] Yang, L.L., Liu, G.R., Zheng, M.H., Jin, R., Zhu, Q.Q., Zhao, Y.Y., Wu, X.L., Xu, Y., 2017. Highly Elevated Levels and Particle-Size Distributions of Environmentally Persistent Free Radicals in Haze-Associated Atmosphere. Environ Sci Technol 51, 7936–7944.
[57] Kiruri L.W. 2013. Experimental and Computational Studies of Environmentally Persistent Free Radicals (EPFRs) Formation, 2013.
[58] Wang, Y.Q., Li, S.P., Wang, M.M., Sun, H.Y., Mu, Z., Zhang, L.X., Li, Y.G., Chen, Q. C., 2019. Source apportionment of environmentally persistent free radicals (EPFRs) in $PM_{2.5}$ over Xi'an, China. Sci Total Environ 689, 193–202.
[59] Xiao, K., Li, L., Zhang, Y.Q., Zhou, Y.S., Fu, D.L., Luo, Z.H., Huang, T.Y., Lu, S.L., Liu, F.W., Lu, J.K., Wang, Q.Y., Shen, G.F., 2024. Environmentally persistent free radicals from residential raw coal combustion and association with chemical components. Emerg Contam 10, 100346.
[60] Li, Q.Q., Dai, L.W., Wang, M.J., Su, G.J., Wang, T.Y., Zhao, X., Liu, X.H., Xu, Y.L., Meng, J., Shi, B., 2022. Distribution, influence factors, and biotoxicity of environmentally persistent free radical in soil at a typical coking plant. Sci Total Environ 835, 12.
[61] Ai, J., Qin, W.H., Chen, J., Sun, Y.W., Yu, Q., Xin, K., Huang, H.Y., Zhang, L.Y., Ahmad, M., Liu, X.A., 2023. Pollution characteristics and light-driven evolution of environmentally persistent free radicals in $PM_{2.5}$ in two typical northern cities of China. J Hazard Mater 454, 131466.
[62] Zhao, X.Q., Tang, L., Zhang, S., Wang, J., Czech, B., Oleszczuk, P., Minkina, T., Gao, Y.Z., 2024. Formation and biotoxicity of environmentally persistent free radicals in steelworks soil under thermal treatment. J Hazard Mater 467, 133697.
[63] Zhang, Q., Geng, G.N., 2019. Impact of clean air action on $PM_{2.5}$ pollution in China. Sci China-Earth Sci 62, 1845–1846.
[64] Liu, B.Y., Wang, L.L., Zhang, L., Bai, K.X., Chen, X.F., Zhao, G.N., Yin, H.T., Chen, N., Li, R., Xin, J.Y., Wang, Y.S., Sun, Y., Hu, B., 2024. Evaluating urban and nonurban $PM_{2.5}$ variability under clean air actions in China during 2010-2022 based on a new high-quality dataset. Int J Digit Earth 17, 21.
[65] Guo, H.B., Wang, Y.D., Yao, K.X., Zheng, H., Zhang, X.J., Li, R., Wang, N., Fu, H.Y., 2023. The overlooked formation of environmentally persistent free radicals on particulate matter collected from biomass burning under light irradiation. Environ Int 171, 10.
[66] Dugas, T.R., Lomnicki, S., Cormier, S.A., Dellinger, B., Reams, M., 2016. Addressing Emerging Risks: Scientific and Regulatory Challenges Associated with Environmentally Persistent Free Radicals. Int J Environ Res Public Health 13, 573.
[67] Qin, L.J., Yang, L.L., Liu, L., Tong, S.L., Liu, Q., Li, G., Zhang, H.Y., Zhu, W.Y.X., Liu, G.R., Zheng, M.H., Jiang, G.B., 2024. Oxidative potential and persistent free radicals in dust storm particles and their associations with hospitalization. Nat Commun 15, 10827.
[68] Chen, Q.C., Sun, H.Y., Wang, M.M., Wang, Y.Q., Zhang, L.X., Han, Y.M., 2019. Environmentally Persistent Free Radical (EPFR) Formation by Visible-Light Illumination of the Organic Matter in Atmospheric Particles. Environ Sci Technol 53, 10053–10061.
[69] Li, H., Chen, Q.C., Wang, C., Wang, R.H., Sha, T., Yang, X.Q., Ainur, D., 2023. Pollution characteristics of environmental persistent free radicals (EPFRs) and their contribution to oxidation potential in road dust in a large city in northwest China. J Hazard Mater 442, 130087.